Title:
# *In situ* observation of re-lubrication of die–workpiece interface during forging with ram pulsation

Authors:
Ryo Matsumoto[1,*], Yusaku Nakamura[1] and Hiroshi Utsunomiya[1]

* Correspnding author (R. Matsumoto, E-mail: ryo@mat.eng.osaka-u.ac.jp, Tel: +81-6-6879-7500, Fax: +81-6-6879-7500)

Affiliation:
[1] Division of Materials and Manufacturing Science, Osaka University, 2-1 Yamadaoka, Suita 565-0871, Japan

**Abstract**

With the aim of investigating the re-lubrication behavior under ram pulsation, the contact interface between die and workpiece was *in situ* observed during cold forging. For *in situ* observation, the die was partly made of transparent ceramic glass, while the workpiece was used commercially pure aluminum. A microscope and high-speed camera were used for observing and recording the contact interface. For analyzing the lubrication behavior, visibility of polybutene lubricant was enhanced by oil-soluble black colorant, and the brightness value of the observed image was used. Obtained results indicated that the lubricant was thickened by approximately 1–10 μm at each ram pulsation through the ram retreat movement in forging with complete unloading ram pulsation. The re-lubrication behavior during ram pulsation was discussed by the thickness of the lubricant, forming load, deformation, and surface roughness of the workpiece.

Keywords: Forging; Extrusion; Lubrication; *In situ* observation; Ram pulsation

## 1. Introduction

Press machines with flexible and accurate ram movements are attractive tools for developing innovative metal forming processes. In hydraulic and mechanical servo presses, the ram movements are realized by servo-drive technology [1]. The plastic flow and temperature of the work material are controlled during forming by the ram operation. The ram operation such as hold, pendulum, stepwise, and pulsation (oscillation) ram motions contributes to shortening of the forming cycle, reducing the forming load, improving the lubrication, and enhancing the shape and dimensional accuracy of the formed product [2].

The ram pulsation (oscillation, vibration, and pulse) was devised through the development of the servo press. In ram pulsation, the ram is repeatedly moved forward (advance) and backward (retreat) at a frequency below approximately 100 Hz and an amplitude over approximately 0.1 mm. The vibration is classified as very low frequency, compared to that of ultrasonic vibration. The work material is loaded and unloaded repeatedly, and deformed intermittently between dies which synchronize with the pulsating ram. Unique forming characteristics appear due to dynamic change in the contact state of the die and the work material. Control of temperature distribution of the work material, control of elastic deformations of the die and the work material, and improvement of lubrication were reported. The enhancement of the shape accuracy of the forged work material was reported in cold backward extrusion-forging [3,4]. This was due to temperature diffusion of local plastic heat generation in the work material during ram pulsation. Further, the influence of ram pulsation conditions on the microscopic grain and macroscopic deformations were reported in cold upsetting of titanium alloy [5] and low carbon steel [6].

Concerning the improvement of lubrication by the ram pulsation, sequential supply of lubricant (re-lubrication) through the gap formed between the die and the work material is essential. The improvement of lubrication and reduction of forming load were realized in

plate compression with load pulsation [7]. The gap was formed at the outer edge of the die–work material contact interface with the elastic recovery of the die and the work material. This technique was applied to plate forging [8] and backward extrusion-forging with internal spline [9]. Friction and forming load were reduced in spline shaft forging with stroke pulsation by the re-building of lubricant film during ram retreat [10]. Galling was reduced in backward extrusion-forging with stroke pulsation by sequentially introducing lubricant to the die–work material interface with negative pressure [11]. The above lubrication technique with negative pressure was applied to improve sheared edge of thick plate in punching with stroke pulsation [12]. Further, other mechanism of lubrication improvement indicated that the ram pulsation assisted to drag the trapped lubricant from the lubricant pockets at the die–work material contact interface. For example, forming load and scratches on the surface of the formed work material were reduced in clutch hub forming with stroke pulsation by dragging the trapped lubricant from the pockets [13].

The die wear with ram pulsation was mainly discussed by the finite element simulation in spline shaft forging [14], backward extrusion-forging [15], and sliding compression test [16]. Predicted by the Archard's wear model [17], the die wear was strongly affected by the forming conditions as well as the ram pulsation. This is because the reductions in friction and contact pressure, together with the increase in sliding distance, occurred at the die–work material contact interface in forming with pulsation ram. Further investigations on the influence of the ram pulsation on the die wear are required.

The reduction mechanisms of friction and forming load by the ram pulsation were investigated through experimental, numerical, and theoretical approaches. The load reduction was numerically investigated in spline shaft forging with ram pulsation using the finite element analysis, along with appropriate friction coefficient and kinematic hardening model of stress-strain relationship of the work material [18]. The load reduction was also

numerically investigated in spline shaft forging with ram pulsation using the finite element analysis, together with the IFUM friction model, and taking into consideration the elastic deformation of the die [19]. Oscillating T-shape compression test with continuous re-lubrication was developed for evaluating the frictional behavior by experiment and finite element simulation [20]. The reduction in friction coefficient was identified by simply comparing the extruded lengths of the work material obtained through the experiment and the finite element simulation in combined forward-backward extrusion-forging with stroke pulsation [21].

*In situ* (direct) observation of the contact interface between die and work material during forming is essential in investigating the tribological phenomena. A well-known technique is as follows: a transparent glass is locally used in the die for observation window, and the glass–work material contact interface is observed from the back side of the glass with a camera during forming. Due to fragility of glass compared to die materials such as tool steel, the *in situ* observation using glass die is limited to steady plastic deformation of work material under low forming pressure. For example, contact behavior between quartz glass die and commercially pure aluminum strip was *in situ* observed during drawing [22]. Entrapment and escape of liquid lubricant were *in situ* observed during drawing of aluminum alloy strip [23]. Introduction of lubricant to the interface of crystal glass roll and commercially pure aluminum strip was *in situ* observed during flat rolling [24]. Lubricant flow between quartz glass die with micro dimples and stainless steel sheet was *in situ* observed during micro bending and ironing [25].

On the other hand, *in situ* observation using glass die for unsteady plastic deformation under high forming pressure such as forging and extrusion is limited to upsetting with slow speed and low reduction in height. For example, trapping of liquid lubricant between quartz glass die and commercially pure aluminum workpiece was *in situ* observed

during upsetting [26,27]. Contact and deformation of OFHC copper workpiece were *in situ* observed using sapphire glass die during micro upsetting [28]. On the other hand, re-lubrication behavior during forging with ram pulsation has not been *in situ* observed using glass die. Recent developments of mobile device displays have resulted in wide circulation of inexpensive high-strength glasses. They may be applied to *in situ* observation for contact interface with dynamic and unsteady plastic deformation such as forging with ram pulsation.

In this study, the contact interface between transparent glass die and commercially pure aluminum workpiece is *in situ* observed during forging with ram pulsation. The lubrication behavior at the contact interface was analyzed by the brightness value of the observed image. Further, the re-lubrication behavior of the workpiece during ram pulsation is discussed by the estimated thickness of the lubricant, forming load, deformation, and surface roughness of the workpiece.

## 2. Forging conditions

### 2.1. Forging shape

**Figure 1** shows the schematic illustrations of the layout and the major dimensions of the die and workpiece for *in situ* observation. The initial shape of the workpiece for forging was cylindrical with 20.0 mm in outer diameter, 10.0 mm in inner diameter and 54.0 mm in height. The bottom end was 13.5 mm in outer diameter, and the section of 0–13.0 mm in the height direction from the bottom end was tapered with 28° in cone angle.

The upper die had a hole with 20.0 mm in diameter and 10.0 mm in depth in the horizontal center for fixing the upper section of the workpiece. The lower die had a combined tapered and straight hole with a square cross-section. Each side of the square cross-section of the tapered section was 21.0 mm on the top side and 12.5 mm on the lower side. The cone angle and depth of the tapered hole were 28° and 17.0 mm in the height direction, respectively.

The lower section of the tapered section was 12.5 mm on each side with the square cross-section. One of the four faces of the tapered section had a stepped hole perpendicular to the tapered surface at a position of 9.0 mm from the top end. The top of the stepped hole was cylindrical with 12.0 mm in diameter and 5.0 mm in depth for fitting the glass, while the bottom of the stepped hole was cylindrical with 4.0 mm in diameter for observing the glass–workpiece contact interface. The lower case had a hole with 6.0 mm in diameter in the same direction with the hole in the tapered section of the lower die from the side. The holes of the lower case and die were straightly connected. The bottom die had a hole with 12.3 mm in diameter for knocking out the workpiece after forging.

The workpiece was forward-extruded from circular cross-section to square cross-section with a reduction in cross-section of 0.63.

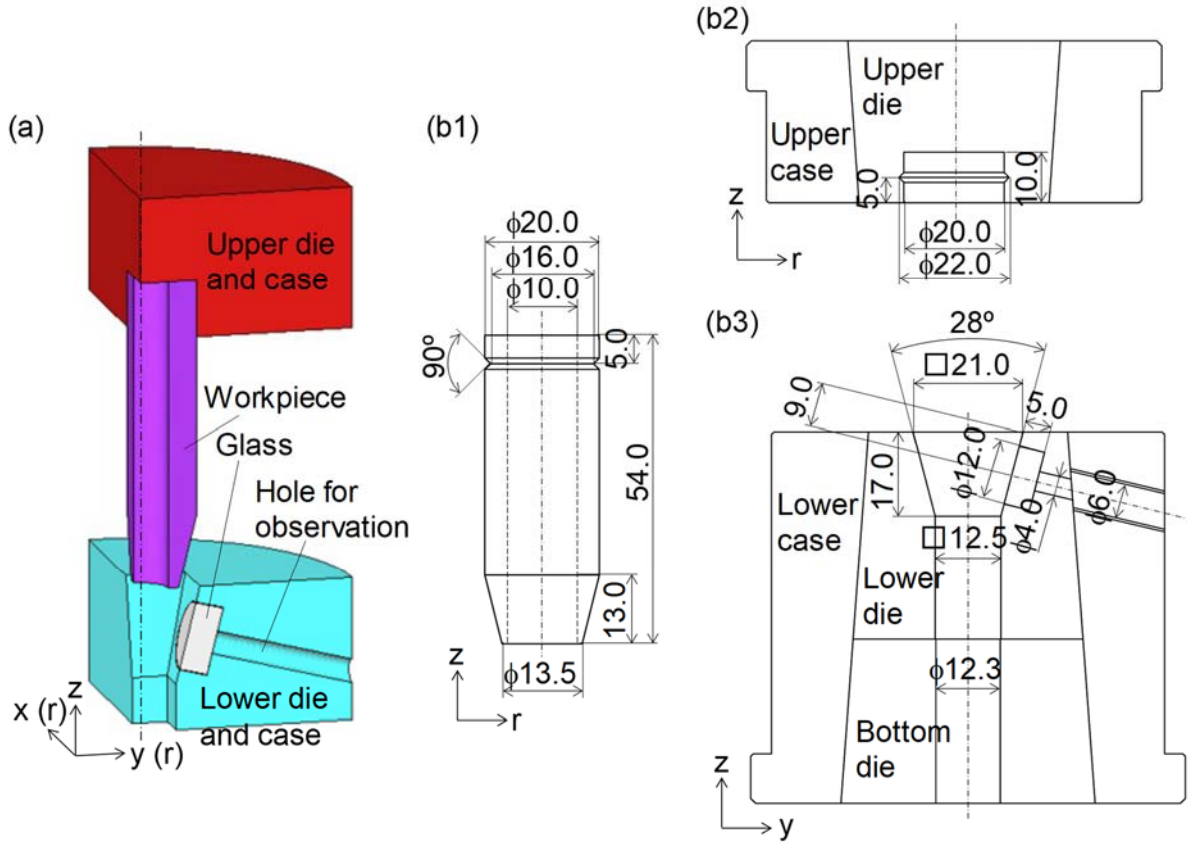


Fig. 1 Schematic illustrations of (a) layout and (b) major dimensions of workpiece and dies, (b1) workpiece, (b2) upper die, and (b3) lower die for *in situ* observation of die–workpiece contact interface during forging.

### 2.2. Press ram motion

**Figure 2** shows the stroke–time diagram of ram pulsation in the second stage of forging. The upper ram of a servo press was operated with combined pulsed and stepwise modes. The workpiece and the upper die were fixed to and thus synchronized with the upper ram. The workpiece was intermittently forward-extruded toward the outlet of the lower die. A gap was formed between the workpiece and the lower die by the ram retreat. During the ram retreat, the workpiece is thereby expected to be re-lubricated by the flow of the lubricant to the gap. To describe the ram motion, $s_{f0}$, $s_{ri}$, $s_{ai}$, and $s_{fi}$ were defined as start stroke of pulsation, retreat stroke, advance stroke, and forming stroke in the $i$-th pulsation ($i$ = 1 to $n_{total}$: total

number of pulsation), respectively.

In this study, $s_{ri}$, $s_{ai}$, and $s_{fi}$ were fixed and constant at every pulsation. Therefore, $s_{ri}$, $s_{ai}$, and $s_{fi}$ can be simply expressed as $s_a$, $s_r$, and $s_f$, respectively. The basic pulsation in this study was set to $s_{f0}$ = 10 mm, $s_r$ = 3 mm, $s_a$ = 4 mm, $s_f$ = 1 mm, and $n_{total}$ = 3 (total forming stroke: $s_{f0} + s_f \cdot n_{total}$ = 13 mm). **Figure 3** shows the relationship between the unload fraction and the retreat stroke in the second stage of forging with ram pulsation. Here, the unload fraction ($\Delta F/F_f$) was defined as follows.

$$\Delta F/F_f = \frac{F_f - F_r}{F_f} \quad (1)$$

where $F_f$ and $F_r$ are the forming loads at start and finish of the ram retreat, respectively. The load was completely unloaded in the case of $\Delta F/F_f$ = 1, while the load was kept to be completely loaded in the case of $\Delta F/F_f$ = 0. The forming load was completely unloaded by the ram retreat with $s_r$ > 1 mm in **Figure 3**. Gap between the workpiece and the lower die was definitely formed by complete unloading. To flow the lubricant to the gap, the retreat stroke was set to $s_r$ = 3 mm in the basic pulsation in this study. Therefore, the maximum gap was formed with approximately 2 mm during the ram retreat with $s_r$ = 3 mm.

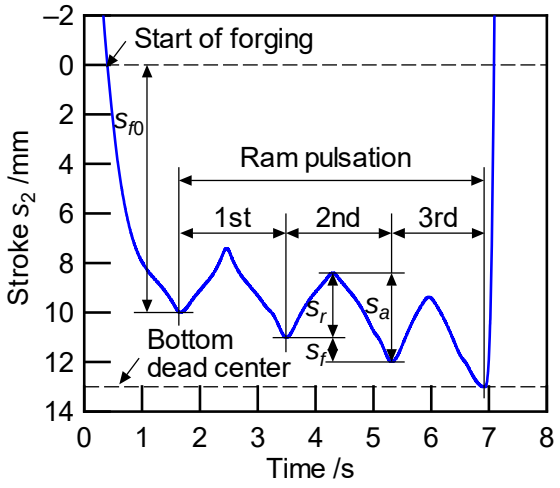


Fig. 2 Stroke–time diagram of ram pulsation in 2nd stage of forging ($s_{f0}$: start stroke of pulsation, $s_r$: retreat stroke in $i$-th pulsation, $s_a$: advance stroke in $i$-th pulsation, $s_f$: forming stroke in $i$-th pulsation).

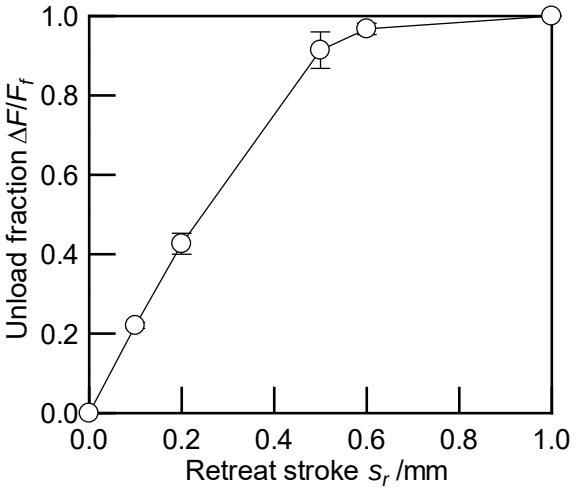


Fig. 3 Relationship between unload fraction and retreat stroke in the second stage of forging.

### 2.3. Experimental conditions

JIS A1070 aluminum drawn bar (Al ≥ 99.7 mass%, Vickers hardness: 36.8 HV0.2) was used as workpiece material for forging. The bar was machined to the cylindrical shape described in Section 2.1 so that the height direction of the workpiece was paralleled with the longitudinal direction of the bar. The surface of the machined workpiece was 0.20–0.50 μm in

arithmetic mean roughness (*Ra*). In addition, a v-shaped notch with 4.0 mm in width and 2.0 mm in depth was machined at a position of 5.0 mm in the height direction from the top end (see **Figure 1(b1)**). The same notch was prepared at a position of 5.0 mm in the height direction from the bottom end of the upper die (see **Figure 1(b2)**). The workpiece was fixed to the upper die at the notches via a rubber o-ring with 17.5 mm in inner diameter and 1.5 mm in wire diameter. Therefore, the movement of the workpiece was synchronized with the upper die and ram in the same manner as described in Section 2.2.

The upper die was two-part structure at each 180° in the circumferential direction parallel to the height direction at the center of the radial (horizontal) direction, while the lower die was five-part structure with each tapered surface (each 90° in the circumferential direction) and two divided tapered surfaces for the glass (each 45° in the circumferential direction) parallel to the height direction at the center of the x direction. Due to these structures, the dies and cases were made of pre-hardened steel (Hitachi Metals Tool Steel, Ltd.: HPM1, Rockwell hardness: 40 HRC). The end surfaces of the upper and lower dies and the surface of the tapered surfaces of the lower die were $Ra$ = 0.11 μm ($Rz$ = 1.2 μm) in surface roughness. The wetting angle of water was approximately 99° on the surface of the tapered section of the lower die at room temperature.

The glass for the observation window was made of transparent ceramic glass (Ohara Inc.: NANOCERAM, Vickers hardness: 710 HV, Young's modulus: 80 GPa). The disk-shaped glass with 12.0 mm in diameter and 5.0 mm in thickness was inserted into the tapered section of the lower die. The manufacturing gap and step between the glass and the cavity of the lower die is maximum 0.01 mm in glass–cavity diameter and maximum 0.005 mm in glass–cavity thickness, respectively. The influence of the gap and step on the deformation behavior of the workpiece was assumed to be negligible. The surface roughness of the glass was $Ra$ = 0.03 μm ($Rz$ = 0.4 μm). The wetting angle of water was approximately 55° on the

surface of the glass at room temperature. As for the glass, no scratch marks and cracks occurred during forging in this study.

Forging was performed in two stages at room temperature on a link-type servo press (Komatsu Industrial Corp., H1F45, maximum load capacity: 450 kN). The glass die–workpiece contact interface was *in situ* observed in the second stage of forging. The first stage of forging was performed without lubrication, with forming stroke of $s_1$ = 12 mm and average forming speed of 8.5 mm/s. The hollow workpiece was partly tapered with a rounded square cross-section by pressing against the tapered section of the lower part in the first stage of forging (see **Figure 6(b)**). Since the main deformation direction of the workpiece was the horizontal direction, the lubricant flow at the glass die–workpiece contact interface was inappropriate for observation. The second stage of forging was performed both with and without lubrication, with forming stroke of $s_2$ = 13 mm ($s_1$+$s_2$ = 25 mm) and average forming speed of 9.0 mm/s (without ram pulsation). The pre-formed workpiece was forward extruded toward the lower section of the lower die.

The lubricant was polybutene with kinematic viscosity of 280 $mm^2/s$ at 313 K and density of 0.87 $g/cm^3$. For better visibility, oil-soluble black colorant (Shirado Chemical Works Ltd.: Liquid Black MX) was mixed with the lubricant at 5 vol%. Hereafter, the lubricant with colorant was simply described as lubricant. Before the second stage of forging, the lubricant was manually applied to the tapered section of the workpiece using a syringe. A lubricant film with approximately 80 μm in thickness was formed by determining the application volume of the lubricant from the application area of the workpiece.

### 2.4. Finite element analysis conditions

The validity of the forging shape as described in Section 2.1 was preliminarily investigated by using a commercial three-dimensional finite element analysis code,

DEFORM-3D ver. 12.0.2 (Scientific Forming Technologies Corporation). In the analysis, plastic deformation of the workpiece was calculated under isothermal state by the rigid-plastic finite element method. The dies were treated as rigid bodies under isothermal state. The workpiece was automatically meshed by approximately 27500 tetrahedral 4-node elements with 0.2–2.5 mm in side length. When the interference between the elements was deformed to be longer than 0.7 in the relative length (interferential length/element size), the elements were automatically re-meshed to tetrahedral 4-node elements.

Since the objective of the analysis was preliminary investigations of the changes in the deformation behavior of the workpiece and the load by the friction of the lower die–workpiece contact interface, the flow stress of JIS A1070 aluminum alloy in the built-in database in DEFORM-3D ver. 12.0.2 was employed. The model of the flow stress was isotropic hardening, and the flow stress–strain relationship was numerically fit according to the Swift law as follows:

$$\sigma = 129(\varepsilon + 0.01)^{0.20} \quad \text{[MPa]} \tag{2}$$

**Figure 4** shows the finite element analysis model. A quarter part of the xy cross-section of the workpiece was analyzed with the consideration of the geometrical symmetry of the forging shape. The dimensions of the workpiece and the dies were identical with those in the experiment as described in Section 2.1. The upper die was moved in the -z direction at a constant 10 mm/s without retreating (no ram pulsation). The observation hole in the lower die and the v-shaped notches in the workpiece and the upper die were not prepared in the analysis. Instead of the v-shaped notch, the contact surfaces of the workpiece and the hole in the upper die was fixed (no sliding) as the boundary condition. The shear friction law was adopted with the consideration of the forging conditions. On assumption of the shear friction law, the shear friction factors were set to 0.4 for the bottom face of upper die–workpiece contact interface and the top face of lower die–workpiece contact interface.

This was considered that the lubricant was applied on the tapered section of the workpiece before forging. On the other hand, the shear friction factor was set to $m$ = 0–0.8 at the constant for the lower die–workpiece contact interface. The influence of the shear friction factor on the forging characteristics was investigated. The change in the friction state during forging was not considered in the analysis because the change in the shear friction factor during forging was difficult to be explicitly identified. Hence, the shear friction factors were set to be constant.

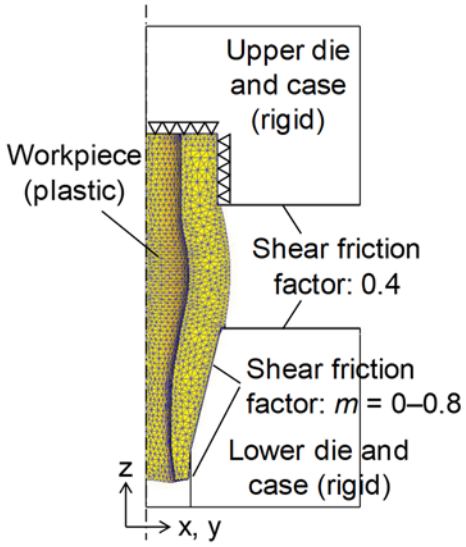


Fig. 4 Cross-sectional view of finite element analysis model for forging (forming stroke in 2nd stage of forging: $s_2$ = 0 mm).

## 3. Observation and image analysis conditions

**Figure 5** shows the appearances of the apparatus for *in situ* observation of the glass die–workpiece contact interface in forging. The contact interface was observed through a straight hole (minimum diameter: 4.0 mm) from the outside of the lower case, through an optical lens and barrel. The glass die–workpiece contact interface was recorded by a high-speed camera (Ditect Co., Ltd.: HAS-U2). The barrel was connected to a white LED

light source (Selmic Corporation: SE-SLED).

The imaging area and resolution were 3.0 mm × 4.0 mm and 600 pixels × 800 pixels in the parallel x horizontal directions with the tapered surface in the lower die, respectively. Since the minimum diameter of the observation hole in the lower die was 4.0 mm as shown in **Figure 1(b3)**, the corner parts of the captured image were the stepped part of the observation hole. The magnification of the lens was 80×, and the shutter speed and frame rate of the camera were set to 1/1000 s and 200 fps, respectively. The light source was set to 2.36 × $10^4$ lx.

The RGB value was converted to the brightness value ($Y$ = 0 (black) to 255 (white)) for each pixel point in the observed color image of the glass die–workpiece contact interface by the following conversion formula.

$$Y = 0.299R + 0.587G + 0.114B \quad (3)$$

where $R$, $G$, and $B$ were the unsigned integers (0–255). The brightness of the lubricant with the oil-soluble black colorant was low, while that of the aluminum workpiece was high. Therefore, it was assumed that the thickness of the lubricant ($t_L$) was thin as the brightness value increased. The relationship between the brightness value and the thickness of the lubricant was approximated by the following formula according to the Beer–Lambert law [29].

$$t_L = \frac{1}{A}\ln\left(\frac{Y}{B}\right) \quad [\mu m] \quad (4)$$

where $A$ and $B$ are constants. The constants of $A$ and $B$ were determined from the experimentally measured results of the relationship between the brightness value and the thickness of the lubricant (see **Figure 19**).

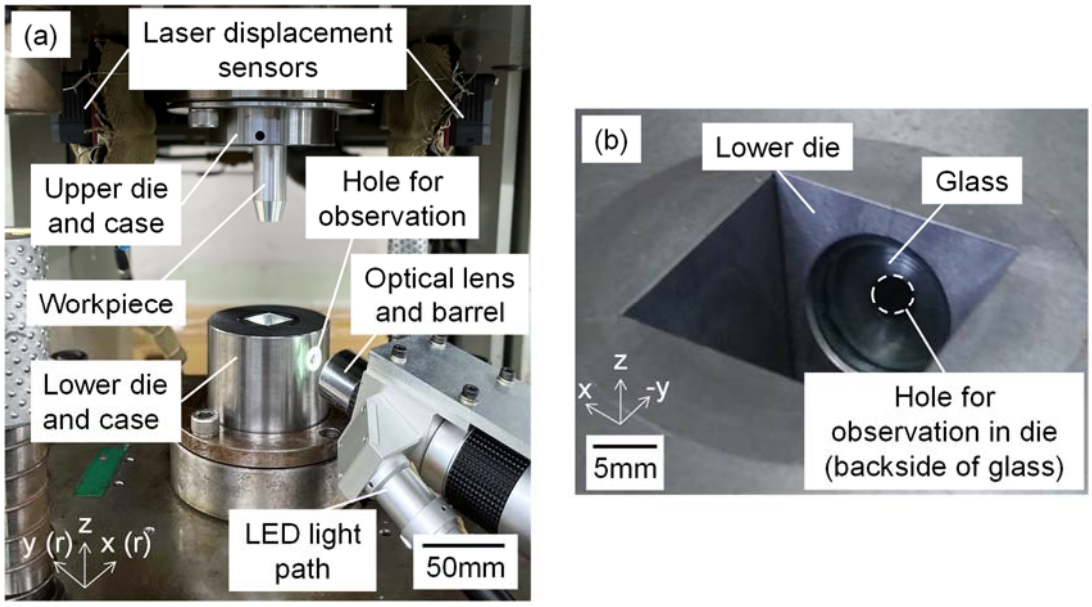


Fig. 5 Appearances of (a) apparatus for *in situ* observation and (b) glass inserted into tapered section of lower die.

## 4. Finite element analysis results of deformation behavior

**Figure 6** shows the finite element analysis results for the deformation of the workpiece in forging. Here, the dark sections of the workpiece were the contact surface with the die. The hollow workpiece was partly tapered from the circular cross-section to the rounded square cross-section in the first stage of forging, and the workpiece hardly extruded in the forward direction. The workpiece was mainly tapered from the circular cross-section to the rounded square cross-section, and hardly extruded in the forward direction in the first stage of forging. In the second stage of forging, the workpiece was forward extruded with the square cross-section and horizontally flanged between the bottom of the upper die and the top of the lower die. In the tapered section of the lower die, the main direction of the deformation of the workpiece was to the horizontal direction in the first stage of forging, while it was to the height direction in the second stage of forging.

**Figure 7** shows the finite element analysis results of the forward length, the flange diameter of the workpiece, and the forming load in the second stage of forging. Due to the

combination of forward extrusion and flange forming, the length, the diameter, and the load increased as the stroke increased. In addition, the difference in each factor between $m$ = 0.2 and 0.8 increased as the stroke increased. Further, the flow volume of the workpiece in the flange section was larger than that of in the forward section, especially at high shear friction factor at lower die–workpiece contact interface. **Figure 8** shows the finite element analysis results of the changes in the forged shape of the workpiece and the forming load with respect to the shear friction factor at lower die–workpiece contact interface in the second stage of forging. As the friction decreased, the forged workpiece had long forward and small flange sections, and the forming load was low during forging.

From the above results, the lubrication state of the lower die–workpiece contact interface in this forging shape was confirmed to be reflected in the deformation behavior of the workpiece and the forming load. The lubrication state could be discussed not only by the observation of the die–workpiece contact interface but also by the shape of the forged workpiece and the forming load. Therefore, the second stage of forging was selected for *in situ* observation of the die–workpiece contact interface. Furthermore, the maximum contact pressure of the tapered section of the lower die in the second stage of forging was approximately 200 MPa in the finite element analysis. As described in Section 2.3, the glass was not expected to break by the forming pressure, taking into consideration the strength of the glass material.

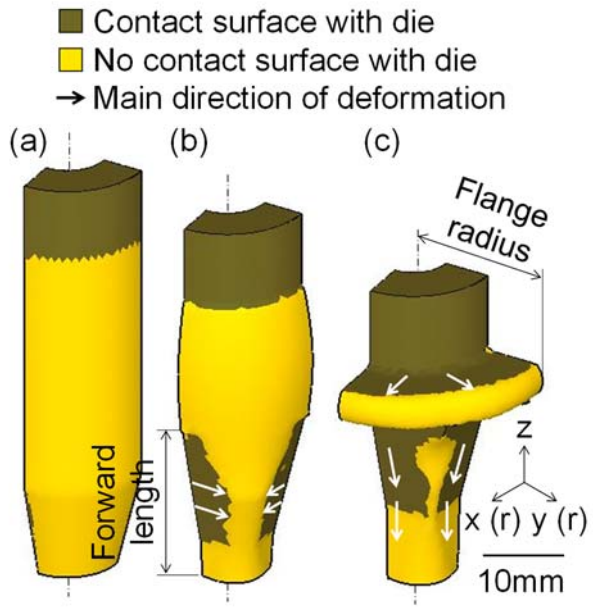


Fig. 6 Deformation of workpiece and contact surface with die in forging (FEM, shear friction factor at lower die–workpiece contact interface: $m$ = 0.2): (a) initial (forming stroke in 1st stage of forging: $s_1$ = 0 mm), (b) end of 1st stage of forging ($s_1$ = 12 mm, forming stroke in 2nd stage of forging: $s_2$ = 0 mm), and (c) end of 2nd stage of forging ($s_2$ = 13 mm).

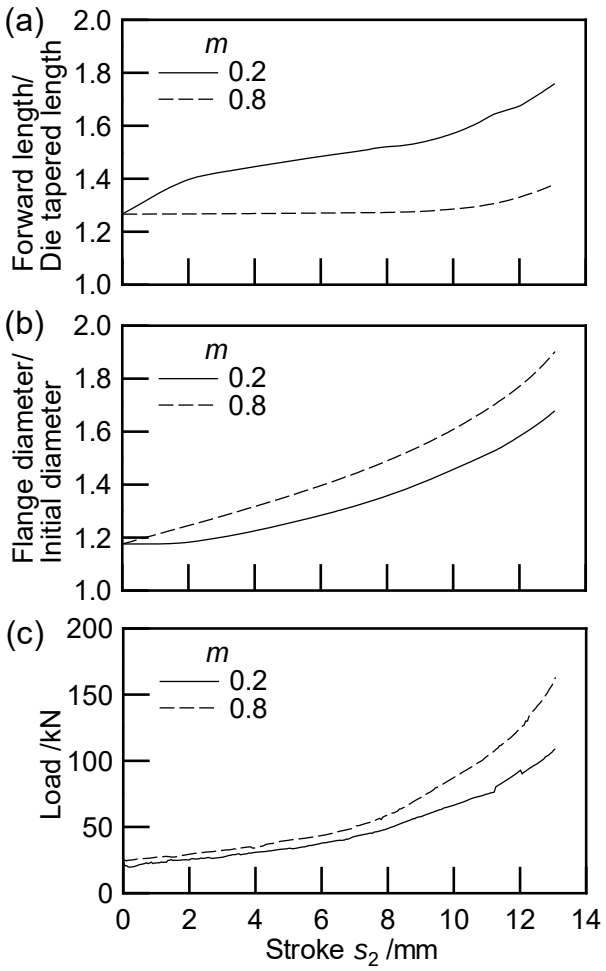


Fig. 7 (a) forward length, (b) flange diameter, and (c) forming load in 2nd stage of forging without ram pulsation (FEM).

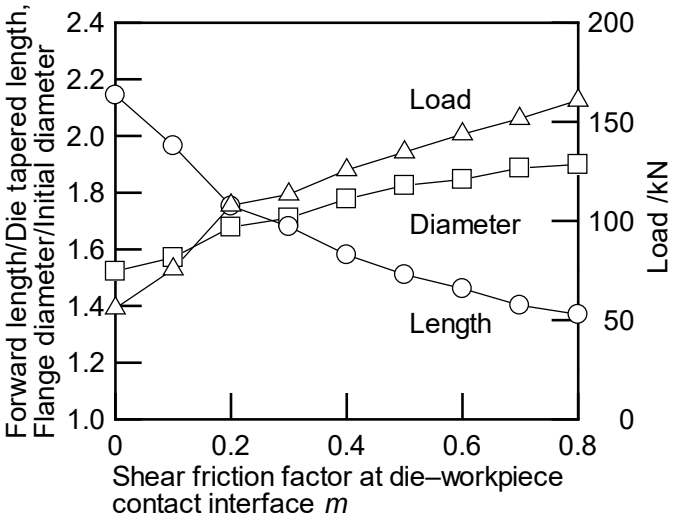


Fig. 8 Changes in shape of forged workpiece and forming load with respect to shear friction factor at lower die–workpiece contact interface in 2nd stage of forging without ram pulsation ($s_2$ = 13 mm, FEM).

## 5. Experimental results

### 5.1. *In situ* observed image and brightness value

**Figure 9** shows the *in situ* observed images of the glass die–workpiece contact interface without ram pulsation. The brightness was not uniform in each image. Due to luster of the aluminum workpiece, sectional halation occurred in the images in forging without lubricant. The brightness was low at the corner parts of the image because the corner parts were captured the stepped part of the observation hole. **Figure 10** shows the *in situ* observed images of the glass die–workpiece contact interface with ram pulsation. Here, the images at the beginning of the ram retreat (before the detachment from the glass die) and the re-forging of the workpiece (after the re-contact to the glass die) are also shown at each ram pulsation ($s_2$ = 10, 11, and 12 mm). The images prior to the beginning of the pulsation ($s_2 \leq$ 10 mm) were similar with the images without ram pulsation (**Figures 9 and 10**). The brightness of the images with lubricant during ram pulsation ($s_2$ = 10–13 mm) was slightly lower than that of the images with lubricant without ram pulsation (**Figures 9 and 10**).

The mean brightness value ($Y_{mean}$) of each image in **Figures 9 and 10** is plotted against the stroke in **Figure 11**. Here, the calculated area for the brightness value was 3.0 mm × 3.0 mm in the center of each image because the corner parts of each image were captured the stepped part of the observation hole as mentioned in Section 3. Due to luster and original color of the aluminum workpiece, the brightness value in forging without lubricant was approximately 250. In contrast, the brightness value with lubricant was much lower. The brightness value in forging with lubricant decreased as the stroke increased at $s_2 \leq 10$ mm, while it sharply increased as the stroke increased at $s_2$ = 10–13 mm without ram pulsation. On the other hand, the brightness value with ram pulsation slightly decreased at every ram retreat ($s_2$ = 10, 11, and 12 mm), and the increase of the brightness value was smaller than that of without ram pulsation. The decrease in the brightness value at $s_2$ = 10, 11, and 12 mm with ram pulsation could indicate the re-lubrication of the glass die–workpiece contact interface by created gap between the glass die and the workpiece.

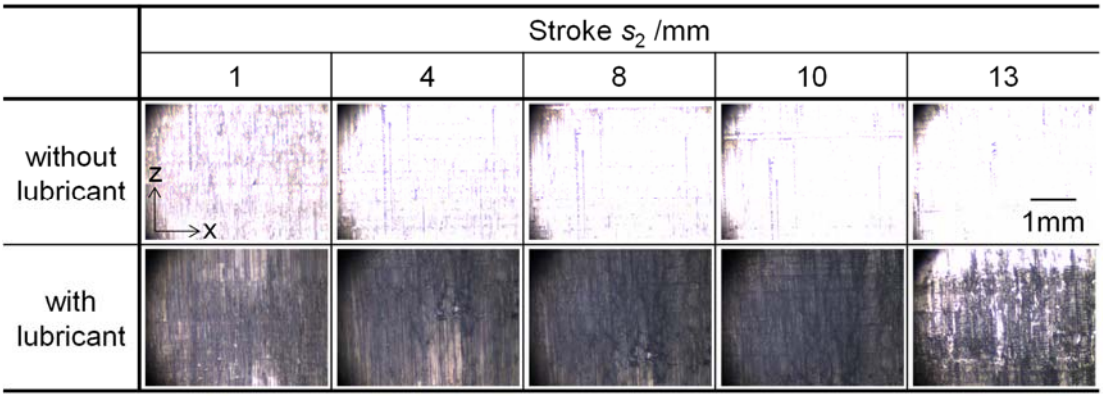


Fig. 9 *In situ* observed images of glass die–workpiece contact interface during forging without ram pulsation.

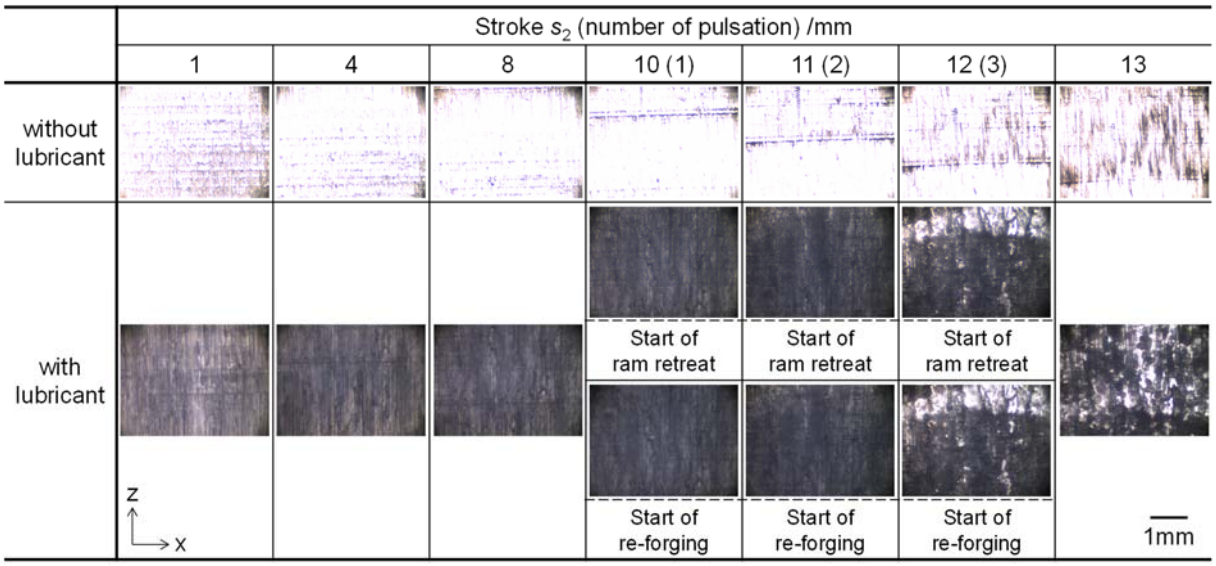


Fig. 10 *In situ* observed images of glass die–workpiece contact interface during forging with ram pulsation.

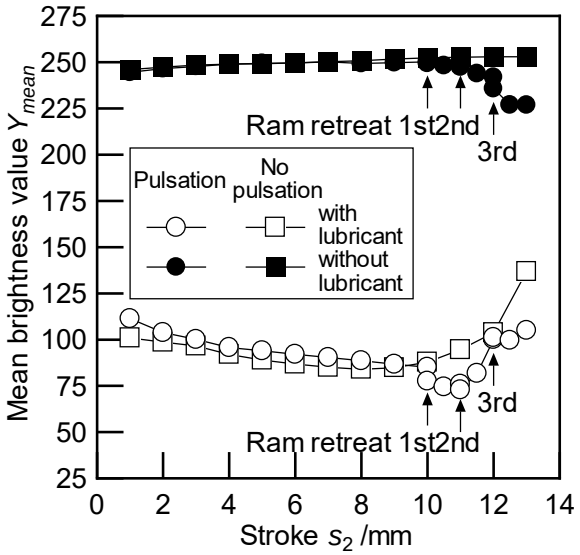


Fig. 11 Mean brightness value of *in situ* observed images of glass die–workpiece contact interface during forging.

### 5.2. Deformation of workpiece and forming load

**Figure 12** shows the measurement results for the shape of the forged workpiece. Here, the forward length (see **Figure 6**) of the forged workpiece was divided by the tapered

length of the lower die in the height direction (17.0 mm). The forward and flange sections of the forged workpiece with lubricant were longer and smaller than those of the forged workpiece without lubricant. The workpiece with lubricant was especially deformed to a long forward section in forging with ram pulsation. **Figure 13** shows the comparison of the forward length of the workpiece forged with the glass and the steel lower dies. The forward length forged with the glass die was slightly shorter than that of with the steel die. The deformation behavior of the workpiece is generally affected by the die material, however, the influence of the die material on the deformation behavior of the workpiece is assumed to be small.

The measurement results of the forming load–stroke curves in the second stage of forging are shown in **Figure 14**. Due to the combination of formation of the flange section and work hardening of the workpiece, the load increased as the stroke increased. In forging with ram pulsation, the load was completely unloaded by the ram retreat at each pulsation ($s_2$ = 10, 11, and 12 mm). Hence the gap between the lower die and the workpiece was formed as predicted in Section 2.2. The load with lubricant was overall lower than that of without lubricant. Note that the load with lubricant during ram pulsation ($s_2$ = 10–13 mm) was reduced by approximately 10–30%, compared to the load without ram pulsation.

From the above obtained results, the lubrication state between the lower die and the workpiece could be evaluated by the forged shape and the forming load. In forging with lubricant with ram pulsation, re-lubrication at lower die–workpiece contact interface is expected to be realized through flowing and re-positioning of the lubricant into the gap between the lower die and the workpiece which is made by the ram retreat during ram pulsation.

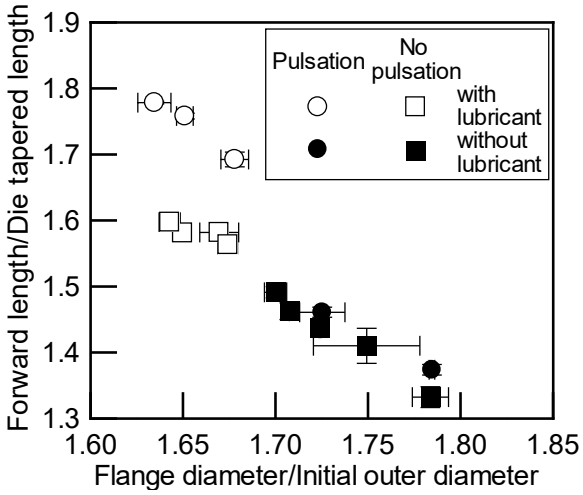


Fig. 12 Shape of forged workpiece ($s_2$ = 13 mm).

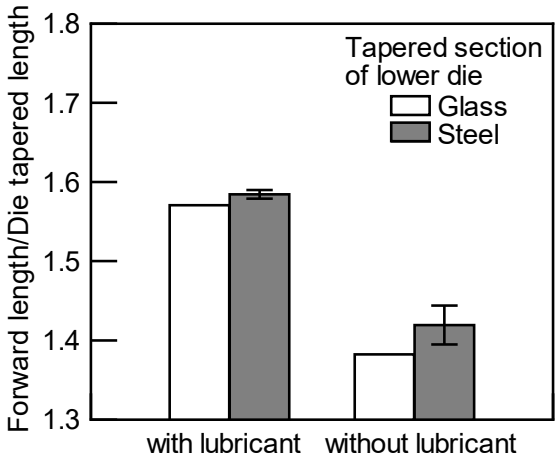


Fig. 13 Comparison of forward length of workpiece forged with glass and steel lower dies without ram pulsation ($s_2$ = 13 mm).

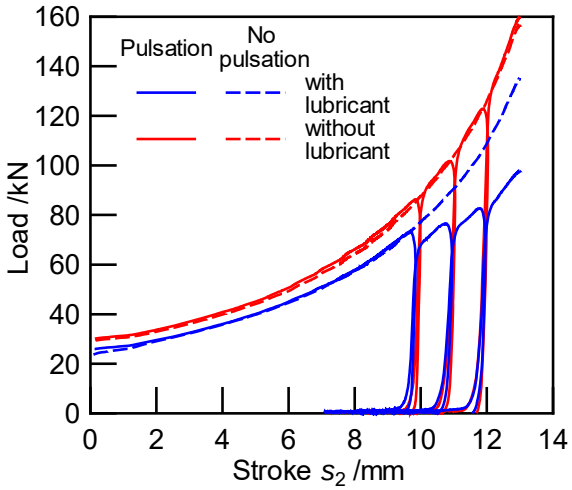


Fig. 14 Forming load–stroke curves in 2nd stage of forging.

### 5.3. Surface photograph and roughness of forged workpiece

**Figure 15** shows the surface photographs of the forged workpiece. The surface conditions of the forged workpiece were almost the uniform in the contact surface with the tapered section of the lower die, especially the contact surface with the glass. **Figure 16** shows the measurement results of the surface roughness of the forged workpiece against the stroke. Here, the surface roughness was measured in the horizontal direction at the contact surface with the glass die. The surface roughness without lubricant was maintained relatively constant during forging with/without ram pulsation, while the surface roughness with lubricant increased as the stroke increased. Notably, the surface roughness with lubricant sharply increased during ram pulsation ($s_2$ = 10–13 mm). The measurement results of the surface profile of the forged workpiece are shown in **Figure 17**. Here, adhesion of the workpiece on the glass die was slightly observed in all forging conditions, although seizure did not occur at the surface of the forged workpiece.

It is concluded from the surface profile that the increase in the surface roughness occurred from lubricant pockets in which the lubricant was trapped at the lower die–workpiece contact interface. Note that due to ram pulsation, the larger amount of the lubricant was trapped at lower die–workpiece contact interface by re-lubrication.

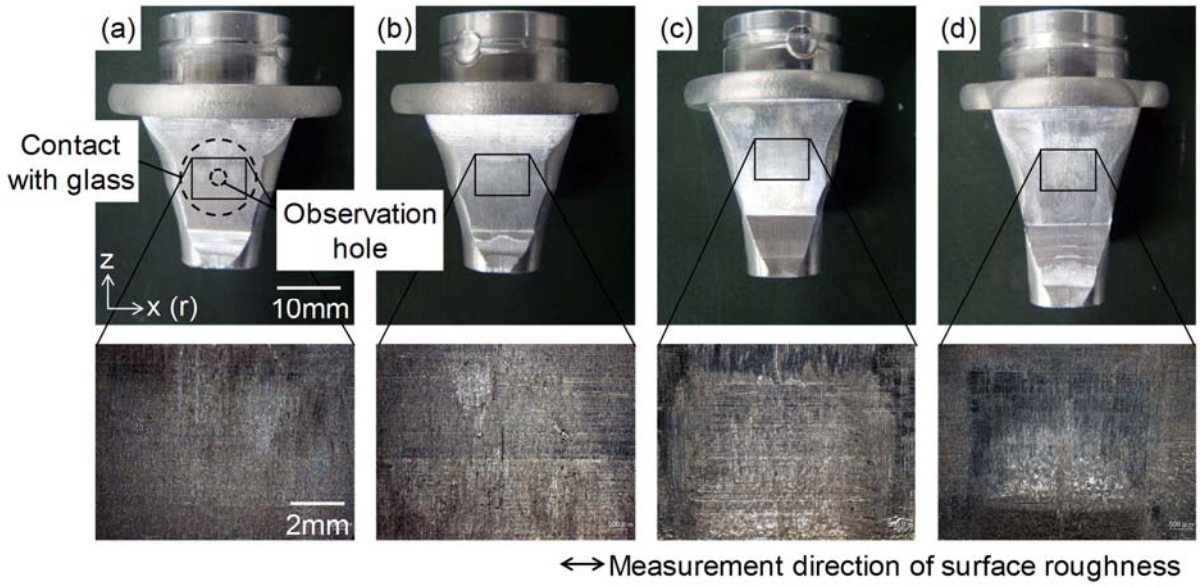


Fig. 15 Surface photographs of forged workpiece ($s_2$ = 13 mm): (a) no pulsation without lubricant, (b) pulsation without lubricant, (c) no pulsation with lubricant, and (d) pulsation with lubricant.

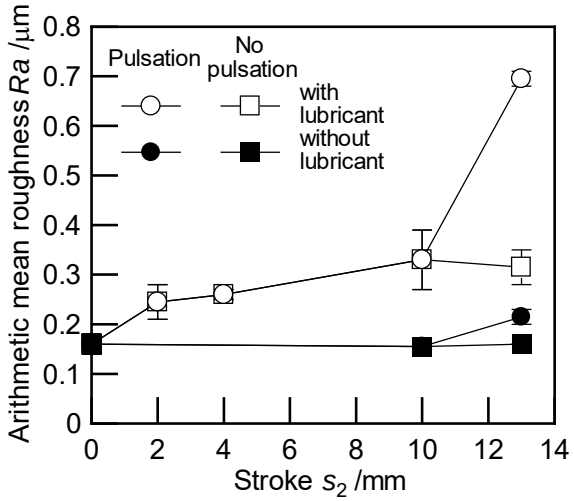


Fig. 16 Surface roughness of contact surface with glass die in forged workpiece.

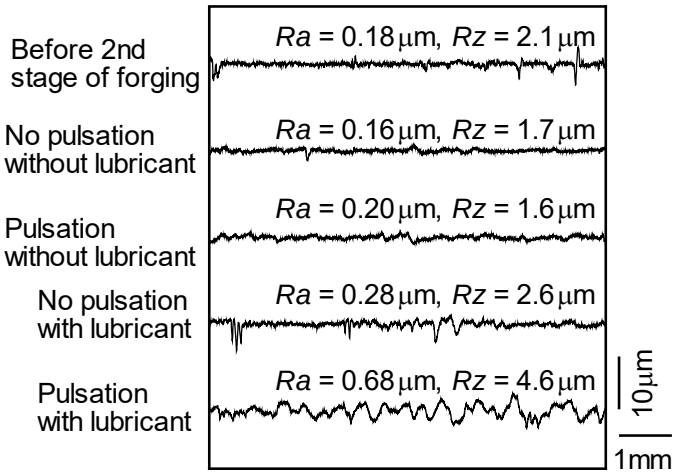


Fig. 17 Surface profile of contact surface with glass die in forged workpiece ($s_2$ = 13 mm).

## 6. Discussions

### 6.1. Thickness of lubricant

To estimate the thickness of the lubricant from the *in situ* observed image of the glass die–workpiece contact interface, the brightness value of the surface of the workpiece applied with the lubricant with $t_L$ = 0–80 μm was measured at each thickness of the lubricant. Here, the thickness of the lubricant was controlled by the applied volume of the lubricant and the applied surface of the workpiece. The thickness of the applied lubricant was assumed to be uniform on the surface of the workpiece. The forged aluminum workpieces with *Ra* = 0.16, 0.28, and 0.68 μm were used. The workpiece inserted into the lower die was observed through the hole of the lower die from the outside of the lower case. The conditions of the camera and the light source were the same as those of the *in situ* observation (see Section 4). The observed images of the glass die–workpiece contact interface without lubricant during and after forging are shown in **Figure 18**. Here, the surface roughness of the aluminum workpiece was *Ra* = 0.16 μm. Although the completely same images were not obtained due to the difference in the contact pressure, the similar images were obtained.

**Figure 19** shows the experimental relationship between brightness value of the observed image of the workpiece with lubricant and the thickness of the applied lubricant. The brightness value decreased as the thickness and the surface roughness of the workpiece increased. However, the difference of the brightness values in $Ra$ = 0.28 and 0.68 μm was small. The experimental relationships were fit by **Equation (4)** as follows.

$$t_L = -\frac{1}{0.021}\ln\left(\frac{Y}{198}\right) \quad (Ra = 0.16\ \mu m) \qquad [\mu m] \qquad (5)$$

$$t_L = -\frac{1}{0.016}\ln\left(\frac{Y}{125}\right) \quad (Ra = 0.28 \text{ and } 0.68\ \mu m) \qquad [\mu m] \qquad (6)$$

On the basis of the measurement results of the surface roughness of the forged workpiece with lubricant, the surface roughness was in the range of $Ra$ = 0.25–0.70 μm (**Figure 16**). **Equation (6)** was used for estimating the thickness of the lubricant from the *in situ* observed image of the glass die–workpiece contact interface. The estimated mean thickness ($t_{L\text{-}mean}$) of the lubricant during forging is shown in **Figure 20**. The mean thickness was estimated from the mean brightness value in **Figure 11**. Here, the thickness was treated as $t_L$ = 0 μm for $Y \geq 125$ because the thickness was $t_L < 0$ μm for $Y \geq 125$ in **Equation (6)**. Because the lubricant was extruded outside of the imaging area at a very early stage of forging, the mean thickness was much thinner than the initial thickness (approximately 80 μm), and increased as the stroke increased at $s_2 \leq 10$ mm. This is because the lubricant was trapped between the lower die and the workpiece during forging. Especially the trapped thickness was gradually thickened at the center part of the tapered section (*in situ* observed area). On the other hand, the mean thickness without ram pulsation sharply decreased as the stroke increased at $s_2$ = 10–13 mm. This is because the lubricant was stretched between the lower die and the workpiece during forging. The mean thickness with ram pulsation was thickened by approximately 1–10 μm at every ram retreat ($s_2$ = 10, 11, and 12 mm); however, the thickness was sharply thinned during ram advancement ($s_2$ = 11–12 mm and 12–13 mm).

**Figure 21** shows the change in the mean thickness of the lubricant against time from the start of the ram retreat to the re-start of forging (the re-contact to the lower die) during the first pulsation. The mean thickness was estimated from the mean brightness value of the *in situ* observed image of the glass die–workpiece contact interface. When the workpiece was detached from the glass die by the ram retreat ($s_r$ > approximately 1 mm), the *in situ* observed image was the lubricant on the surface of the glass die. The lubricant was nominally thinned during the ram retreat at $s_r$ > approximately 1 mm, since the lubricant was split between the surfaces of the glass die and the workpiece. Compared with the thicknesses at the start of the ram retreat to the re-start of forging, the lubricant was thickened by approximately 1–10 μm as described above. The reduction of friction at the lower die–workpiece contact interface as described in Section 5.2 was realized through re-lubrication of the workpiece caused by the increase in the thickness of the lubricant.

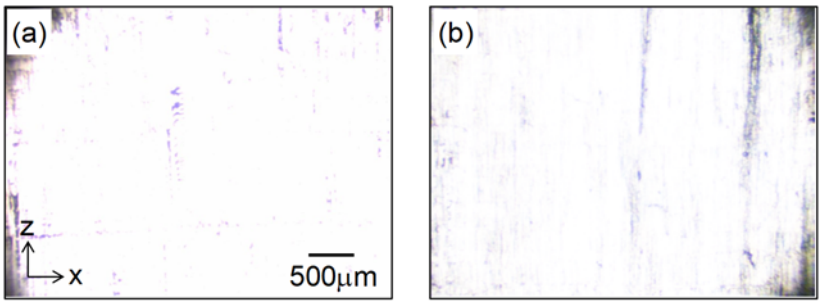


Fig. 18 Observed images of glass die–workpiece contact interface without lubricant (surface roughness of workpiece: *Ra* = 0.16 μm): (a) during forging without pulsation and (b) after forging ($s_2$ = 13 mm).

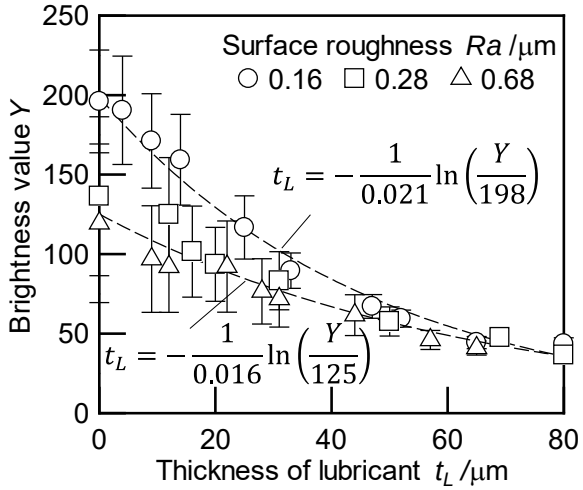


Fig. 19 Experimental relationship between brightness value of observed image of workpiece with lubricant and applied thickness of lubricant at glass die–workpiece contact interface.

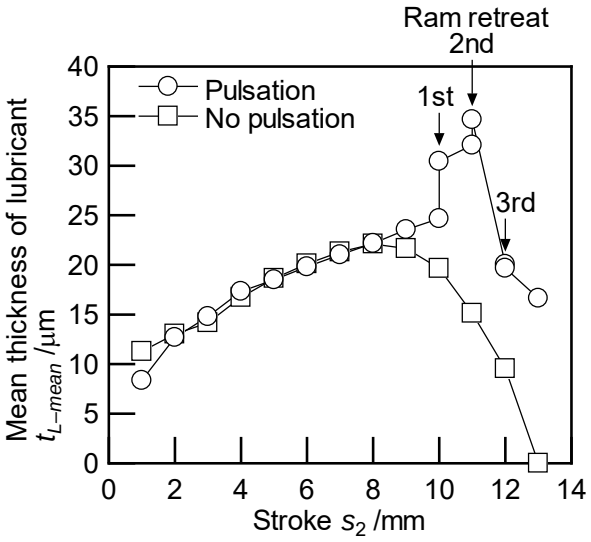


Fig. 20 Estimated mean thickness of lubricant at glass die–workpiece contact interface during forging with lubricant.

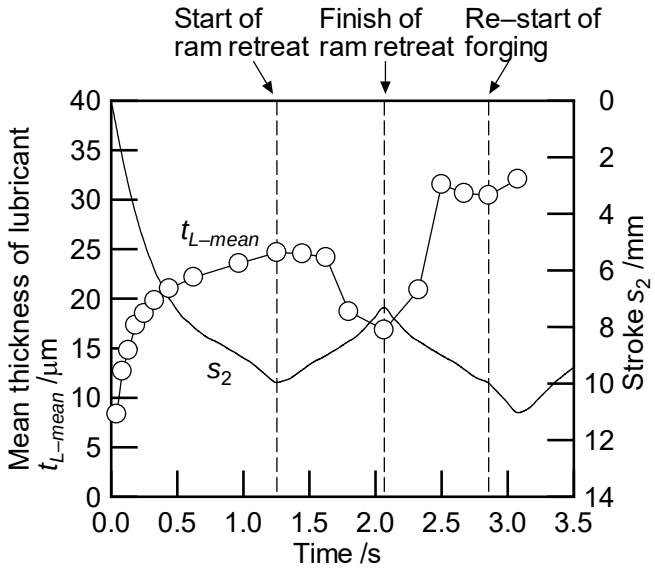


Fig. 21 Estimated mean thickness of lubricant at glass die–workpiece contact interface during ram pulsation at $s_2$ = 10 mm in forging with lubricant.

### 6.2. Re-lubrication mechanism

To discuss the lubrication mechanism during ram pulsation, the influence of the retreat stroke of the ram on the thickness of the lubricant at glass die–workpiece contact interface was investigated. Here, the ram pulsations were set to $s_{f0}$ = 10 mm, $s_r$ = 0–3 mm, $s_f$ = 3 mm, and $n_{total}$ = 1. In addition, the ram was to hold for two seconds at the end position of the ram retreat. Since the forming load was completely unloaded by the ram retreat with $s_r$ > 1 mm as described in Section 2.2, the gap between the lower die and the workpiece was not formed at $s_r$ < 1 mm. **Figure 22** shows the estimated mean thickness of the lubricant during forging. Compared with the thicknesses at the start of the ram retreat and the re-start of forging at each pulsation, the lubricant was thickened in the ram pulsation with $s_r$ = 3 mm. Next, the forming load–stroke curves in the ram pulsations are shown in **Figure 23**. The load was completely unloaded at the end of the ram retreat with $s_r$ = 3 mm, while the load was unloaded by approximately 60% at the end of the ram retreat with $s_r$ = 0.3 mm. The load was kept to be reduced by approximately 10% during re-forging ($s_2$ = 10–13 mm) in the ram

pulsation with $s_r$ = 3 mm, while the load in the ram pulsation with $s_r$ = 0.3 mm was almost the same in no ram pulsation ($s_r$ = 0 mm) during re-forging. In partial unloading with $s_r$ < 1 mm, the gap was formed at the edge of the die–workpiece contact interface; however, the gap and the area were not enough for reducing the load.

The thickening of the lubricant during ram pulsation with complete unloading was expected to be caused by the combination of (a) the flow of the lubricant into the observed area (center of the tapered sections of the workpiece and the lower die) and (b) re-positioning of the lubricant film. The illustration of the lubricant flow at the die–workpiece contact interface in the tapered section of the lower die during ram pulsation with complete unloading is shown in **Figure 24**. The lubricant trapped at the die–workpiece contact interface is split between the surfaces of the die and the workpiece during the ram retreat before complete unloading ($\Delta F/F_f$ < 1, **Figure 24(b)**). After complete unloading ($\Delta F/F_f$ = 1, **Figure 24(c)**), the lubricant applied before forging and squeezed during forging on the upper outer surface of the workpiece flows to the observed area of the workpiece through the gap between the die and the workpiece. The lubricant flow is expected to be caused due to the ram movement and the viscosity of the lubricant. Then the lubricant is re-positioned and thickened by contacting between the lubricant on the surface of the die and the lubricant on the surface of the workpiece during ram advance (**Figure 24(d)**). The lubricant flows in **Figure 24(b), (c), and (d)** correspond to the thickness change in the lubricant in 1.3–1.7 s, 1.7–2.3 s, and 2.3–2.8 s in **Figure 21**, respectively.

From the above results and discussions, it is concluded that the complete unloading and the formation of the gap between the lower die and the workpiece are required for the increase of the thickness of the lubricant and the reduction of the load during the ram pulsation with lubricant.

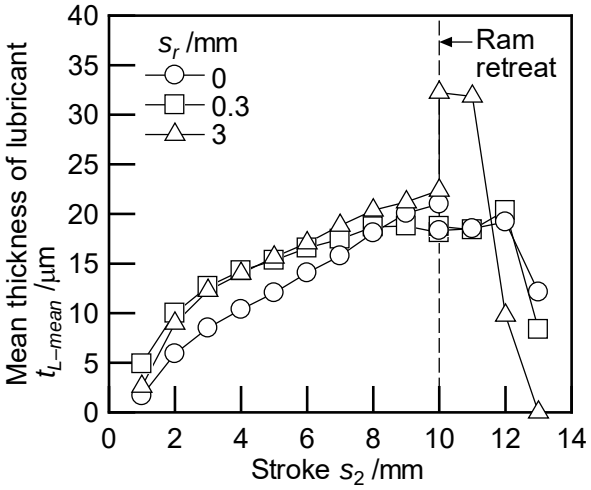


Fig. 22 Estimated mean thickness of lubricant at glass die–workpiece contact interface during forging with ram pulsations of $s_{f0}$ = 10 mm, $s_r$ = 0–3 mm, $s_f$ = 3 mm, and $n_{total}$ = 1.

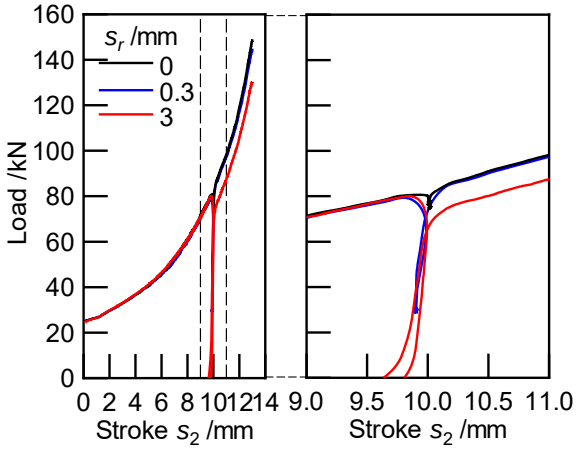


Fig. 23 Forming load–stroke curves in forging with ram pulsations of $s_{f0}$ = 10 mm, $s_r$ = 0–3 mm, $s_f$ = 3 mm, and $n_{total}$ = 1.

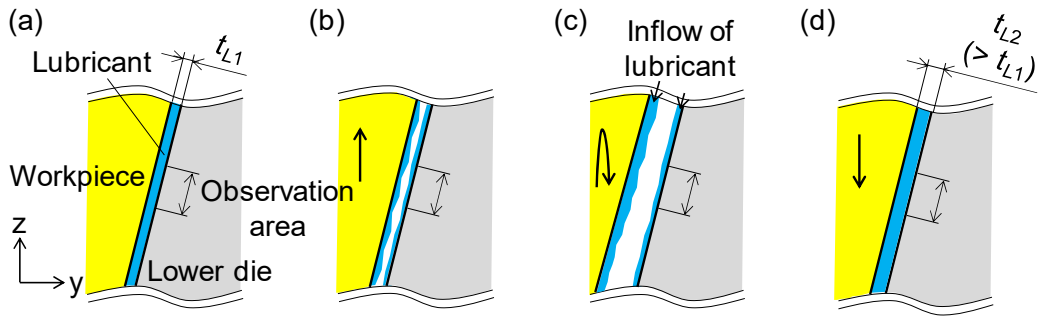


Fig. 24 Illustration of lubricant flow at die–workpiece contact interface on tapered section of lower die during ram pulsation with complete unloading: (a) Start of ram retreat ($\Delta F/F_f = 0$), (b) During ram retreat ($\Delta F/F_f < 1$), (c) During ram retreat and advance ($\Delta F/F_f = 1$), and (d) During ram advance (just before re-start of forging).

## 7. Conclusions

In this study, the contact interface between transparent glass die and aluminum workpiece was *in situ* observed during forging with ram pulsation. The lubrication behavior at the contact interface was analyzed by the brightness value of the observed image. The re-lubrication behavior of the workpiece during ram pulsation was discussed by the estimated thickness of the lubricant, forming load, deformation, and surface roughness of the workpiece. The following conclusions were obtained.

(1) Mixing approximately 5 vol% of oil-soluble black colorant into the polybutene (lubricant) enhanced the visibility of the lubricant on the aluminum workpiece. With the colorant, the thickness of the lubricant could be easily estimated by measuring the brightness value.

(2) In forging with complete unloading ram pulsation, the lubricant was analyzed to be thickened by approximately 1–10 μm between the start of the ram retreat and the re-start of forging at each pulsation. Measurements were obtained through the change in the mean brightness of the *in situ* observed images.

(3) Owing to the increase of the lubricant at each ram pulsation, the workpiece was

re-lubricated in forging with complete unloading ram pulsation. The re-lubrication was confirmed by the reduction in forming load, the change in the shape of the forged workpiece, and the formation of the lubricant pockets on the surface of the forged workpiece.

(4) In forging conditions of this study, re-lubrication during ram pulsation was realized under complete unloading ram pulsation (retreat stroke of longer than 1 mm). The gap was formed between the die and the workpiece by the ram retreat. The lubricant was thickened at the surfaces of the die and the workpiece by flowing and re-positioning between the start of the ram retreat and the re-start of forging at each pulsation.

**Acknowledgements**

This work was financially supported in part by the Japan Society for the Promotion of Science (JSPS) with a Grant-in-Aid for Scientific Research (C) (19K05097) and the Die and Mould Technology Promotion Foundation.

**References**

1) Yadav A, Kaya S, Groseclose A, Electromechanical servo-drive presses. Sheet Metal Forming: Fundamentals (Altan, T. and Tekkaya, A.E. eds.). ASM International 2012; 161–180. https://doi.org/10.31399/asm.tb.smff.t53400161
2) Osakada K, Mori K, Altan T, Groche P. Mechanical servo press technology for metal forming. CIRP Annals – Manufacturing Technology 2011; 60(2): 651–672. https://doi.org/10.1016/j.cirp.2011.05.007
3) Matsumoto R, Jeon JY, Utsunomiya H. Shape accuracy in the forming of deep holes with retreat and advance pulse ram motion on a servo press. Journal of Materials Processing Technology 2013; 213(5): 770–778. https://doi.org/10.1016/j.jmatprotec.2012.11.023

4) Ishikawa T, Ishiguro T, Yukawa N, Goto T. Control of thermal contraction of aluminum alloy for precision cold forging. CIRP Annals – Manufacturing Technology 2014; 63(1): 289–292. https://doi.org/10.1016/j.cirp.2014.03.008

5) Lin J, Pruncu C, Zhu L, Li J, Zhai Y, Chen L, Guan Y, Zhao G. Deformation behavior and microstructure in the low-frequency vibration upsetting of titanium alloy. Journal of Materials Processing Technology 2022; 299: 117360. https://doi.org/10.1016/j.jmatprotec.2021.117360

6) Meng D, Ma J, Zhao X, Guo Y, Zhu C, Yu M. Mechanical behavior and material property of low-carbon steel undergoing low-frequency vibration-assisted upsetting. Journal of Materials Research and Technology 2022; 16: 1846–1855. https://doi.org/10.1016/j.jmrt.2021.12.113

7) Maeno T, Osakada K, Mori K. Reduction of friction in compression of plates by load pulsation. International Journal of Machine Tools and Manufacture 2011; 51(7-8): 612–617. https://doi.org/doi: 10.1016/j.ijmachtools.2011.03.007

8) Maeno M, Mori K, Hori A. Application of load pulsation using servo press to plate forging of stainless steel parts. Journal of Materials Processing Technology 2014; 214(7): 1379–1387. https://doi.org/10.1016/j.jmatprotec.2021.117360

9) Maeno M, Mori K, Ichikawa Y, Sugawara M. Use of liquid lubricant for backward extrusion of cup with internal splines using pulsating motion. Journal of Materials Processing Technology 2017; 244: 273–281. https://doi.org/10.1016/j.jmatprotec.2017.02.001

10) Groche P, Heß B. Friction control for accurate cold forged parts. CIRP Annals – Manufacturing Technology 2014; 63(1): 285–288. https://doi.org/10.1016/j.cirp.2014.03.012

11) Matsumoto R, Sawa S, Utsunomiya H, Osakada K. Prevention of galling in forming of

deep hole with retreat and advance pulse ram motion on servo press. CIRP Annals – Manufacturing Technology 2011; 60(1): 315–318. https://doi.org/10.1016/j.cirp.2011.03.147

12) Maeno T, Sugawara M, Saito T, Terada A, Mori K. Improvement of burnished area in punching of stainless steel thick plate by means of pulsating motion. Procedia Manufacturing 2020; 50: 203–209. https://doi.org/10.1016/j.promfg.2020.08.038

13) Meng D, Zhu C, Zhao X, Zhao S. Applying low-frequency vibration for the experimental investigation of clutch hub forming. Materials 2018; 11: 928. https://doi.org/10.3390/ma11060928

14) Schmidt W, Groche P. Wear prediction for oscillating gear forming processes using numerical methods. Key Engineering Materials 2018; 767: 283–289. https://doi.org/10.4028/www.scientific.net/KEM.767.283

15) Matsumoto R, Utsunomiya H. Punch wear in the forming of deep holes with pulse ram motion on a servo press. Key Engineering Materials 2014; 611-612: 127–133. https://doi.org/10.4028/www.scientific.net/KEM.611-612.127

16) Groche P, Schmidt W. Wear prediction in oscillating cold forging processes. Tribology Letters 2020; 68: 128. https://doi.org/10.1007/s11249-020-01367-w

17) Archard JF. Contact and rubbing of flat surfaces. Journal of Applied Physics 1953; 24(8): 981–988. https://doi.org/10.1063/1.1721448

18) Heß B, Ubelacker D, Groche P. Numerical investigation on the force reduction in axial forming by oscillating ram movement. Proceedings of the 6th JSTP International Seminar on Precision Forging 2013; 89–92.

19) Zhang Q, Ben NY, Yang K. Effect of variational friction and elastic deformation of die on oscillating cold forging for spline shaft. Journal of Materials Processing Technology 2017; 244: 166–177. https://doi.org/10.1016/j.jmatprotec.2017.01.001

20) Ben N, Zhang Q, Bandyopadhyay K, Lee MG. Analysis of friction behaviour under oscillating forming process using T-shape compression test and finite element simulation. Journal of Materials Processing Technology 2020; 275: 116327. https://doi.org/10.1016/j.jmatprotec.2019.116327

21) Matsumoto R. Hayashi K, Utsunomiya H. Experimental and numerical analysis of friction in high aspect ratio combined forward-backward extrusion with retreat and advance pulse ram motion on a servo press. Journal of Materials Processing Technology 2014; 214(4): 936–944. https://doi.org/10.1016/j.jmatprotec.2013.11.017

22) Azushima A. Direct observation of contact behavior to interpret the pressure dependence of the coefficient of friction in sheet metal forming. CIRP Annals – Manufacturing Technology 1995; 44(1): 209–212. https://doi.org/10.1016/S0007-8506(07)62309-9

23) Bech J, Bay N, Eriksen M. Entrapment and escape of liquid lubricant in metal forming. Wear 1999; 232(2): 134–139. https://doi.org/10.1016/S0043-1648(99)00136-2

24) Ike H, Tsuji K, Takase M. In situ observation of a rolling interface and modeling of the surface texturing of rolled sheets. Wear 2002; 252(1-2): 48–62. https://doi.org/10.1016/S0043-1648(01)00854-7

25) Shimizu T, Kobayashi H, Vorholt J, Yang M. Lubrication analysis of micro-dimple textured die surface by direct observation of contact interface in sheet metal forming. Metals 2019; 9(9): 917. https://doi.org/10.3390/met9090917

26) Azushima A, Yoneyama S, Yamaguchi T, Kudo H. Direct observation of microcontact behavior at the interface between tool and workpiece in lubricated upsetting. CIRP Annals – Manufacturing Technology 1996; 45(1): 205–210. https://doi.org/10.1016/S0007-8506(07)63048-0

27) Azushima A. In situ 3D measurement of lubrication behavior at interface between tool and workpiece by direct fluorescence observation technique. Wear 2006; 260(3): 243–248.

https://doi.org/10.1016/j.wear.2005.01.053

28) Weidel S, Engel U, Merklein M, Geiger M. Basic investigations on boundary lubrication in metal forming processes by in situ observation of the real contact area. Production Engineering Research and Development 2010; 4(2-3): 107–114. https://doi.org/10.1007/s11740-009-0198-5

29) Verhoeven JW. Glossary of terms used in photochemistry (IUPAC Recommendations 1996). Pure and Applied Chemistry 1996; 68(12): 2223–2286. https://doi.org/10.1351/pac199668122223]